JACS
JOURNAL OF THE AMERICAN CHEMICAL SOCIETY

Article

pubs.acs.org/JACS

Roles of Cooperative Interactions in Graphene Intercalation: Mechanistic Study

Geng Li,[†,#] Haitao Zhou,[†,#] Lida Pan,[†,#] Yi Zhang,[†] Li Huang,[†] Wenyan Xu,[†] Shixuan Du,[†] Min Ouyang,[‡] Andrea C. Ferrari,*[,§] and Hong-Jun Gao*[,†]

[†]Institute of Physics, Chinese Academy of Sciences, Beijing 100190, P.R. China

[‡]Department of Physics and Center for Nanophysics and Advanced Materials, University of Maryland, College Park, Maryland 20742, United States

[§]Cambridge Graphene Centre, University of Cambridge, Cambridge, CB3 0FA, United Kingdom

Supporting Information

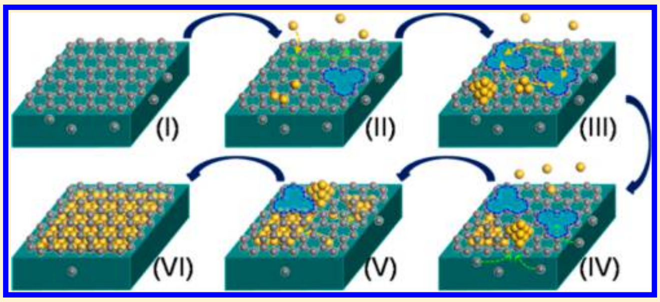

ABSTRACT: Intercalation phenomenon in graphene has arisen substantial interest over the past few years due to its importance of tailoring intrinsic graphene properties as well as creating novel vertical heterostructures. While various graphene intercalation processes have been reported with different combination of foreign atoms and substrates, a thorough atomistic mechanism behind requires additional work. By employing Si intercalation between epitaxially grown graphene and Ru(0001) substrate as a model system, we have performed an in-depth study with elucidation of roles of cooperative interaction that is defined among foreign atoms, graphene, and substrate. By combining scanning tunneling microscopy with density functional calculation, the intercalation process is confirmed to consist of four key steps, involving creation of defects, migration of foreign atoms, self-repairing of graphene, and growth of intact intercalated monolayer. Both theoretical simulation and experiment have demonstrated that this intercalation mechanism can be extended to other systems, thus representing a universal process.

INTRODUCTION

Graphene, a two-dimensional crystal of carbon atoms packed in a honeycomb structure, has manifested many fascinating mechanical,[1] electrical[2,3] and optical properties.[4] In addition to that, graphene can interact with various heteroatoms or molecules to tailor its intrinsic property as well as to create novel hybrid graphene-based heterostructures.[5−18] This offers a new degree of freedom to design functional graphene-based device architectures. Indeed, a variety of atomic[5−13] and molecular[14,15,17] species have been successfully integrated with graphene on substrates via intercalation process. Understanding and maneuvering this intercalation process should thus be critical in realizing novel graphene-based heterostructures.[19,20]

In the present work, by combining atomic scale characterization with density functional theory (DFT) modeling we have investigated the key processes governing the intercalation of heteroatoms between graphene and a substrate. The Si intercalation between a graphene and Ru(0001) is chosen as a test bed according to following considerations: (1) Si plays an important role in electronics, thus development of hybrid graphene-Si structures/devices may offer a seamless integration with current microelectronics industry; and (2) graphene with exceptional quality has been routinely obtained by epitaxial growth method on Ru(0001).[21] Such a defect-free graphene system can ensure a clear understanding of intercalation process without concern of such as pre-existence defects, thus avoiding complication of interpretation. Particularly, we have found that the foreign adatoms, graphene, and substrate are needed to be considered as a whole in order to facilitate intercalation process (i.e., cooperative interaction). Our results should pave the way for large area production of devices based on hybrids between graphene and layers of foreign materials that will be challenging to achieve otherwise.[19,20] Other combination of heteroatoms (such as Ni, Pd and Pt), and substrates (such as Ir(111) and SiC(0001)) are also investigated to support the generality of our study.

EXPERIMENTAL SECTION

Intercalation of Si. Single layer graphene (SLG) was achieved by exposing a Ru(0001) single crystal surface to ethylene at 1300 K.[21] The process was performed in an Omicron low-temperature scanning tunneling microscope (STM) system with a base pressure lower than 1.0×10^{-10} mbar. A current was applied to surface of a thin Si wafer to sublimate Si atoms onto the SLG substrate at room temperature. Calibration was taken by measuring Si deposition onto a clean Ru(0001) surface, where Si can form epitaxial monolayer (ML) islands. Based on STM images of different areas of the sample, a

Received: November 23, 2014

DOI: 10.1021/ja5113657
J. Am. Chem. Soc. XXXX, XXX, XXX−XXX

statistic analysis was taken to measure the average coverage of Si on the Ru(0001) surface. The heating current was fixed, and the deposition amount of Si was thus assumed to be proportional to the evaporation duration. Different deposition amounts can be achieved by carefully adjusting the evaporation duration. The calibration process was repeated more than 10 times to ensure the accuracy. The sample was then annealed at different temperatures to initiate intercalation process.

Ar^+ Ion Bombardment. An Omicron ISE 10 ion source was used to create single vacancy defects on SLG. The density of defects is determined by ion energy, Ar base pressure, filament emission current as well as bombardment duration. In our experiment, we fixed the ion energy at 100 eV, Ar pressure at 3×10^{-6} mbar, and emission current at 0.1 mA and varied the bombardment duration to tune the density of defects.

DFT Calculation. The DFT calculation within the local density approximation[22] was performed using the Vienna ab initio simulation package.[23] The projector augmented wave (PAW)[24] method was used. More details of simulation are provided in the Supporting Information.

■ RESULTS AND DISCUSSION

Figure 1a shows a 90 × 90 nm STM topographic image of graphene after partial intercalation of Si. Before Si intercalation, an intact defect-free SLG is confirmed (see Supporting Information Figure S1).[21] In this figure, its upper right portion shows a smooth and flat feature that can be assigned as SLG/Si/Ru with a Si ML between the SLG and Ru. The rest of image represents a region with a small percentage of Si intercalation, as evidenced by the appearance of small isolated Si islands underneath graphene with a line profile shown in Figure 1b. High-resolution image (Figure 1c) further reveals that the SLG is intact and uniform after the Si intercalation, which is confirmed by both STM characterization at different sample areas and Raman spectroscopy[25] (see Supporting Information Figure S2).

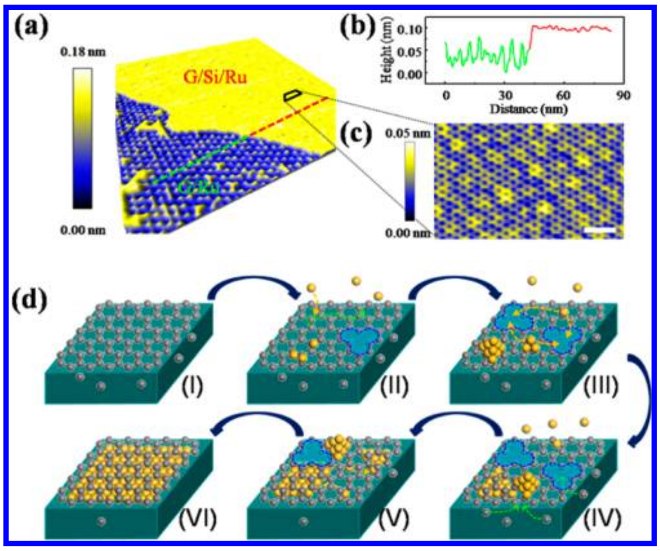

Figure 1. STM topography of SLG/Si/Ru layer and proposed intercalation process. (a) Three- dimensional view of the intercalated Si layer. (b) Height profile along a line depicted in (a). (c) Atomic resolution image showing the graphene lattice on top of the intercalated Si layer in the rectangular area highlighted in (a). The scale bar is 1 nm. (d) Schematic intercalation process. The yellow and green arrows represent diffusion paths of the Si and C atoms, respectively.

A few mechanisms have been proposed to account for similar intercalation processes.[7,11,14,16,18] For example, heteroatoms can diffuse through, such as graphene island edges or pre-existing defects due to reduced intercalation energy barrier,[7,11,14,18] or exchange with carbon atoms.[16] However, none of them can explain our observation: Our SLG is intact with negligible pre-existing defects.[21] Previous low-energy electron microscopy study[16] also suggests that the Si atoms could directly penetrate through SLG without requirement of edges[14] or wrinkles.[18] Furthermore, the temperature utilized in our experiment is relatively low (e.g., 450 °C for Si), which is not enough to break carbon−carbon bond to form defects on graphene (carbon−carbon bonding energy is estimated to be ∼5.67 eV,[26] corresponding to a temperature of $\sim 6.6 \times 10^4$ K) or to enable the Si−C exchange process that requires at least 3 eV energy.[16] To that, a thorough understanding of intercalation process is needed.

Figure 1d outlines our proposed mechanism by highlighting a few key steps: cooperative creation of defects (stage II), migration of heteroatoms through graphene to Ru surface (stage III), self-repair of the graphene lattice (stage IV), and assembly of heteroatoms to form an intercalated layer (stage V). It is worthy to note that these four steps are intercorrelated and can happen simultaneously under certain experimental conditions, which makes it challenging for unambiguous characterization.

Figure 2a shows a typical image of sample after deposition of 0.05 ML Si onto an originally defect-free SLG/Ru surface, followed by annealing at 400 °C for 10 min (results of annealing under lower temperatures can be found in Supporting Information Figure S3). In addition to large bright protrusions that can be assigned to be as-deposited Si clusters,

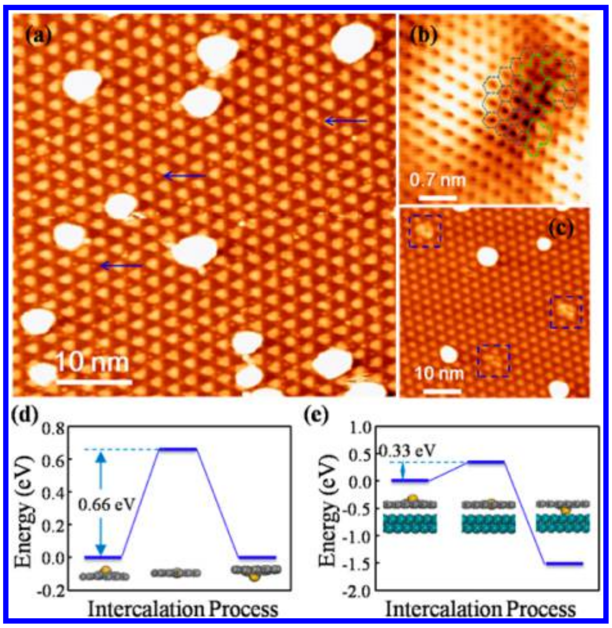

Figure 2. Si-induced defect formation. (a) STM image of SLG/Ru with predeposition of 0.05 ML Si at room temperature, followed by thermal annealing at 400 °C for 10 min. (b) Atomically resolved image revealing the nature of carbon vacancy defect (bias voltage $V_s = -0.1$ V, tunneling current $I_t = 0.3$ nA). (c) STM image of sample in (a) after another thermal annealing at 450 °C for 30 min. (d and e) The predicted energy barrier of Si intercalation without and with Ru substrate, respectively.

many randomly distributed small dot-like features can be identified (some are guided by the blue solid arrows in Figure 2a, see also Supporting Information Figure S4a,b). These small dot-like features can be assigned as carbon vacancies accompanied by distortion of honeycomb lattice, as revealed in high- resolution image (Figure 2b). Another supporting evidence of our assignment of carbon vacancy is that the small dot-like feature revealed in Figure 2a can only be observed at the lower temperature (350 °C ~ 400 °C) within a short time period (~10 min). Under higher temperature and/or with sufficient time (e.g., > 30 min) Si adatoms can migrate, accumulate and combine with carbon vacancies, resulting in small bumps with different apparent height (e.g., feature outlined by dashed squares in Figure 2c). Furthermore, we have performed one important control experiment by heating graphene on the Ru substrate under the same condition without predeposition of Si, but we have not observed any similar vacancy defect features as shown in Figure 2 (Supporting Information Figure S4c). This suggests that the involvement of Si is a prerequisite for defect formation under our experimental conditions.

We further compare defect formation energies of four different scenarios (as listed in Supporting Information Figure S5) by ab initio calculation:[27] free-standing graphene, SLG/Ru, free-standing graphene with a Si adatom, and SLG/Ru with a Si adatom. A substantial energy reduction from 8.09 eV (free-standing graphene) to 0.23 eV (Si-graphene-Ru) is observed after consideration of an interaction among Si adatoms, graphene, and substrate, making it feasible to open carbon vacancy defects under our experimental condition.

The availability of carbon vacancies can thus facilitate migration of Si atoms through the graphene layer. In order to evaluate the role of defects in the intercalation process, we have performed one control experiment by intentionally creating single vacancy defects by low-energy ion bombardment.[28] The argon ions with an energy of 100 eV can create single vacancy defects on SLG/Ru with defect density controllable by changing the dosage and duration (Supporting Information Figures S6 and S7). The same amount (2 ML) of Si is deposited onto SLG/Ru samples with different initial defect density (Supporting Information Figure S6a−c), followed by annealing at 700 °C for 30 min. Our result has shown that the higher initial defect density, the more Si can be intercalated (Supporting Information Figure S6d−f), suggesting that defects indeed enable and promote intercalation and supporting our proposed defect assisted intercalation process.

In order to evaluate the role of substrate in the intercalation process, we have employed the climb nudged elastic band method[29] to simulate migration of a single Si atom through a vacancy defect. Figure 2d,e compares the energy barrier difference for the migration process without and with consideration of the effect of Ru(0001), respectively. We have observed a significant reduction of energy barrier from 0.66 eV (without substrate) to 0.33 eV (with substrate), suggesting that the Ru substrate can further reduce the energy barrier of this process as well as the total energy of the system during the Si intercalation. This effect also makes the inverse process (i.e., migration of Si atoms from the interface to the upper SLG surface) become less likely under our experimental condition.

We have experimentally observed that the honeycomb carbon lattice can be restored after the Si intercalation with the annihilation of carbon vacancy defects in the temperature range from 300 to 800 °C. In order to annihilate vacancy defects, extra carbon atoms are required, which can be originated either from the knockout carbon atoms in the defect formation stage or from the bulk Ru substrate.[30] In particular, we have studied the relationship between the defect density of SLG and the annealing temperature. Figure 3a−c shows three typical STM images of SLG/Ru obtained by annealing at different temperatures of 25, 300, and 450 °C, respectively (same initial defect density as well as annealing time was applied to all samples in this control experiment). The temperature-dependent analysis of defect density is summarized in Figure 3d, showing that the graphene defect density substantially decreases with the increase of temperature. In our experiment, we have observed that the annealing condition of 700 °C for 30 min is enough to repair almost all defects on the SLG surface after the Si intercalation and to recover high-quality graphene lattice. This defect annihilation process is critical in order to create high-quality graphene-based hybrid structures.

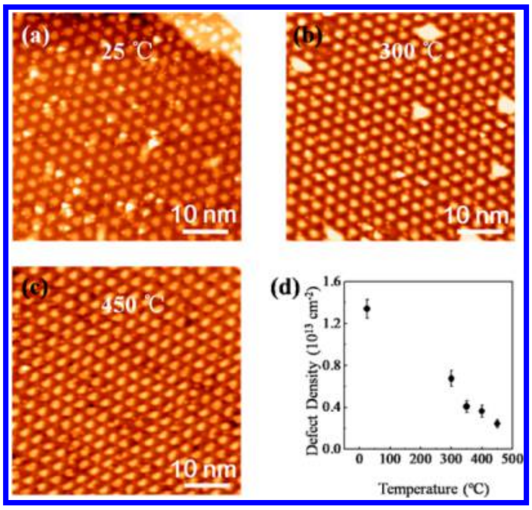

Figure 3. Removal of vacancy defects on SLG/Ru. STM images of the SLG/Ru samples annealed at (a) 25 °C, (b) 300 °C, and (c) 450 °C for 30 min. These samples have the same initial defect density, controlled by argon ion bombardment dosage and duration. (d) Relationship between defect density on SLG/Ru surface and annealing temperature. Each data point with error bar was obtained by averaging defect numbers of eight 50 × 50 nm STM images taken at different sample areas for a given temperature.

We explore the evolution and assembly of the intercalated Si layer (i.e., stages V and VI in Figure 1d). While it was suggested before that the intercalated atoms could diffuse into the metal substrate and form related alloys,[31] we have clearly observed that the Si atoms tend to spread at the interface without the formation of alloy. Figure 4a−c shows the development of three different structures of the intercalated Si layer with the increase of the Si dosage from 0.3 to 0.8 ML. At the very beginning with low coverage, the intercalated Si atoms are found to preferentially migrate and occupy underneath the graphene's atop sites[32] (hills of the moiré structure) (Figure 4a). This is supported by the fact that the intercalated atop sites become enlarged with the topographic distortion from the usual round shape of the pristine graphene (Supporting Information Figure S1). Once all available atop sites are occupied, more incoming Si atoms start occupying face-centered cubic (fcc, medium regions of the moiré structure) and then hexagonal close

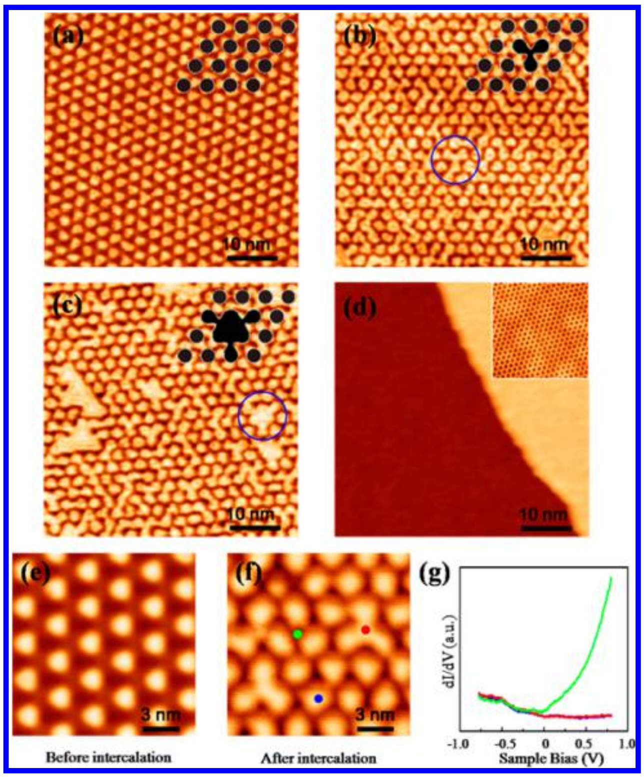

Figure 4. Evolution of the intercalated Si layer between SLG and Ru substrate.The intercalated Si atoms can sequentially occupy the areas below (a) atop sites, (b) fcc sites and (c) hcp sites. The inset shows the corresponding structural configuration of the intercalated Si atoms. (d) Full ML Si is formed at the interface. Inset is a 4.5 nm × 4.5 nm atomic resolution image showing the perfect carbon lattice of graphene after intercalation. (e and f) Typical topography ($V_s = -0.05$ V, $I_t = 1.0$ nA) before and after Si intercalation, respectively. (g) The dI/dV spectra acquired at the different locations marked in (f). The red, blue, and green curves correspond to the dI/dV spectra acquired at the intercalated fcc sites, the intercalated atop sites, and the non-intercalated fcc sites, respectively.

packed (hcp, lowest regions of the moiré structure) sites, leading to the appearance of Y-shaped and triangular structures, as shown in Figure 4b,c, respectively. Once the atop, fcc and hcp sites are fully occupied, a full Si ML underneath the graphene is completed (Figure 4d) with the manifestation of different structural and electronic characteristics. For example, the variation of topographic feature before and after Si intercalation can be found by comparing Figure 4e with 4f. The dI/dV curves measured at the intercalated fcc and atop sites show similar features, but differ from that of the nonintercalated fcc sites (Figure 4f,g). This can be understood as that the electronic structure of graphene becomes decoupled from the substrate after the Si intercalation.

Importantly, we have also performed similar experiments as well as DFT calculations to evaluate and compare different combination of heteroatoms and substrates, with a few examples highlighted in Figure 5. Our DFT computation shows that many different intercalation systems can manifest similar defect opening process with the reduction of defect formation energy (Figure 5a), highlighting the generality of our proposed graphene intercalation mechanism, i.e., the carbon vacancy defects can be created by the interaction among the heteroatoms, the graphene, and the substrate under very mild experimental condition, and the heteroatoms can thus migrate through the carbon defect sites to form an ordered intercalated ML, while the defects of graphene can be annealed to restore its crystalline lattice. Figure 5b−d shows experimental confirmation of similar defect creation process in the intercalation of Ni, Pd, and Pt between SLG and Ru substrate (highlighted by green arrows in Figure 5b−d) as that described for the Si intercalation process.

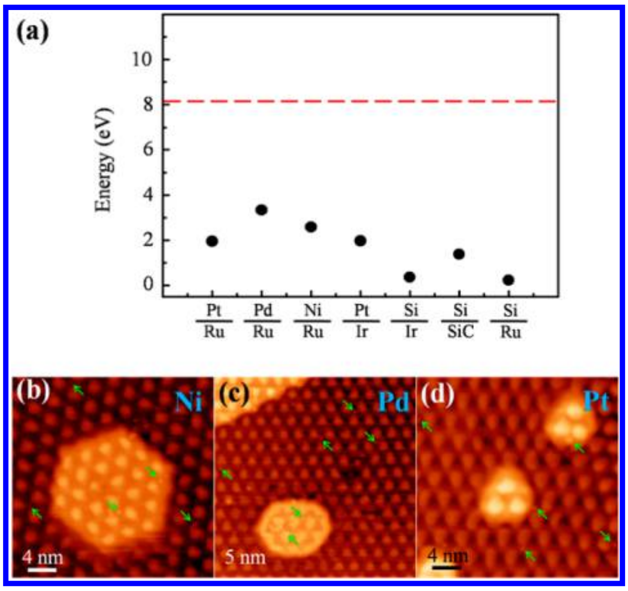

Figure 5. Defects induced by other types of materials during intercalation. (a) Calculated formation energy of single vacancy defects in different graphene intercalating systems. The red dashed line indicates the defect formation energy in a free-standing graphene, and the black dots represent defect formation energies in different intercalating systems. (b−d) STM images showing the SLG/Ru surface after intercalation of Ni, Pd, and Pt. The green arrows highlight the defects created in the intercalation process.

■ CONCLUSIONS

We have presented a mechanistic study with detailed evidence to understand and control the intercalation process of heteroatoms between a graphene layer and the substrate, which is governed by the interplay among the heteroatoms, the graphene, and the substrate. Importantly, such cooperative intercalation can result in both the formation of the large-scale intact intercalated layer and the restoration of perfect graphene lattice at relatively low temperature, which makes it feasible to create vertical graphene-based heterostructures with atomic layer precision and to minimize interfacial roughness. This should be critical for future mass-scale development of the graphene devices, as compared with current layer-by-layer assembly by hand.[19,20]

■ ASSOCIATED CONTENT

Ⓢ Supporting Information

Information and figures regarding the sample preparation and characterization; detailed discussions about DFT calculations and Ar^+ ion bombardment experiments. The Supporting Information is available free of charge on the ACS Publications website at DOI: 10.1021/ja5113657.

■ AUTHOR INFORMATION

Corresponding Authors

*acf26@eng.cam.ac.uk

*hjgao@iphy.ac.cn

Author Contributions

[#]These authors contributed equally.

Notes

The authors declare no competing financial interest.

■ ACKNOWLEDGMENTS

Work at IOP was supported by grants from National Science Foundation of China, National "973" projects of China, the Chinese Academy of Sciences, and SSC. M.O. acknowledged support from the ONR (award no. N000141410328) and the NSF (DMR1307800). A.C.F acknowledges funding from EU Graphene Flagship (contract no. CNECT-ICT-604391), a Royal Society Wolfson Research Merit Award, the European Research Council Grants NANOPOTS, Hetero2D, EU grants GENIUS, MEM4WIN, CareRAMM, EPSRC grants EP/K01711X/1, EP/K017144/1.

■ REFERENCES

(1) Lee, C.; Wei, X.; Kysar, J. W.; Hone. *J. Science* **2008**, *321*, 385−388.

(2) Novoselov, K. S.; Geim, A. K.; Morozov, S. V.; Jiang, D.; Katsenlson, M. I.; Grigorieva, I. V.; Dubonos, S. V.; Firsov, A. A. *Nature* **2005**, *438*, 197−200.

(3) Wu, Y. Q.; Jenkins, K. A.; Valdes-Garcia, A.; Farmer, D. B.; Zhu, Y.; Bol, A. A.; Dimitrakopoulos, C.; Zhu, W.; Xia, F.; Avouris, P.; Lin, Y. M. *Nano Lett.* **2012**, *12*, 3062−3067.

(4) Bonaccorso, F.; Sun, Z.; Hasan, T.; Ferrari, A. C. *Nat. Photonics* **2010**, *4*, 611−622.

(5) Enderlein, C.; Kim, Y. S.; Bostwick, A.; Rotenberg, E.; Horn, K. *New J. Phys.* **2010**, *12*, 033014.

(6) Virojanadara, C.; Watcharinyanon, S.; Zakharov, A. A.; Johansson, L. I. *Phys. Rev. B* **2010**, *82*, 205402.

(7) Jin, L.; Fu, Q.; Mu, R.; Tan, D.; Bao, X. *Phys. Chem. Chem. Phys.* **2011**, *13*, 16655−16660.

(8) Sicot, M.; Leicht, P.; Zusan, A.; Bouvron, S.; Zander, O.; Weser, M.; Dedkov, Y. S.; Horn, K.; Fonin, M. *ACS Nano* **2012**, *6*, 151−158.

(9) Huang, L.; Pan, Y.; Pan, L.; Gao, M.; Xu, W.; Que, Y.; Zhou, H.; Wang, Y.; Du, S.; Gao, H. J. *Appl. Phys. Lett.* **2011**, *99*, 163107.

(10) Mao, J. H.; Huang, L.; Pan, Y.; Gao, M.; He, J.; Zhou, H.; Guo, H.; Tian, Y.; Zou, Q.; Zhang, L.; Zhang, H.; Wang, Y.; Du, S.; Zhou, X.; Castro Neto, A. H.; Gao, H. J. *Appl. Phys. Lett.* **2012**, *100*, 093101.

(11) Xia, C.; Watcharinyanon, S.; Zakharov, A. A.; Yakimova, R.; Hultman, L.; Johansson, L. I.; Virojanadara, C. *Phys. Rev. B* **2012**, *85*, 045418.

(12) Emtsev, K. V.; Coletti, C.; Forti, S.; Starke, U. *Phys. Rev. B* **2011**, *84*, 125423.

(13) Riedl, C.; Coletti, C.; Iwasaki, T.; Zakharov, A. A.; Starke, U. *Phys. Rev. Lett.* **2009**, *103*, 246804.

(14) Sutter, P.; Sadowski, J. T.; Sutter, E. A. *J. Am. Chem. Soc.* **2010**, *132*, 8175−8179.

(15) Feng, X. F.; Maier, S.; Salmeron, M. *J. Am. Chem. Soc.* **2012**, *134*, 5662−5668.

(16) Cui, Y.; Gao, J.; Jin, L.; Zhao, J.; Tan, D.; Fu, Q.; Bao, X. *Nano Res.* **2012**, *5*, 352−360.

(17) Zhao, W.; Tan, P. H.; Liu, J.; Ferrari, A. C. *J. Am. Chem. Soc.* **2011**, *133*, 5941−5946.

(18) Petrović, M.; Šrut Rakić, I.; Runte, S.; Busse, C.; Sadowski, J. T.; Lazić, P.; Pletikosić, I.; Pan, Z.-H.; Milun, M.; Pervan, P.; Atodiresei, N.; Brako, R.; Šokčević, D.; Valla, T.; Michely, T.; Kralj, M. *Nat. Commun.* **2013**, *4*, 2772.

(19) Britnell, L.; Gorbachev, R. V.; Jalil, R.; Belle, B. D.; Schedin, F.; Mishchenko, A.; Georgiou, T.; Katsnelson, M. I.; Eaves, L.; Morozov, S. V.; Peres, N. M. R.; Leist, J.; Geim, A. K.; Novoselov, K. S.; Ponomarenko, L. A. *Science* **2012**, *335*, 947−950.

(20) Haigh, S. J.; Gholinia, A.; Jalil, R.; Romani, S.; Britnell, L.; Elias, D. C.; Novoselov, K. S.; Ponomarenko, L. A.; Geim, A. K.; Gorbachev, R. *Nat. Mater.* **2012**, *11*, 764−767.

(21) Pan, Y.; Zhang, H.; Shi, D.; Sun, J.; Du, S.; Liu, F.; Gao, H. J. *Adv. Mater.* **2009**, *21*, 2777−2780.

(22) Perdew, J. P.; Zunger, A. *Phys. Rev. B* **1981**, *23*, 5048−5079.

(23) Kresse, G.; Furthmuller, J. *Phys. Rev. B* **1996**, *54*, 11169−11186.

(24) Blochl, P. E. *Phys. Rev. B* **1994**, *50*, 17953−17979.

(25) Ferrari, A. C.; Basko, D. M. *Nat. Nanotechnol.* **2013**, *8*, 235−246.

(26) Girit, Ç. Ö.; Meyer, J. C.; Erni, R.; Rossell, M. D.; Kisielowski, C.; Yang, L.; Park, C.-H.; Crommie, M. F.; Cohen, M. L.; Louie, S. G.; Zettl, A. *Science* **2009**, *323*, 1705−1708.

(27) Wang, L.; Zhang, X.; Chan, H. L. W.; Yan, F.; Ding, F. *J. Am. Chem. Soc.* **2013**, *135*, 4476−4482.

(28) Ugeda, M. M.; Brihuega, I.; Guinea, F.; Gómez-Rodríguez, J. M. *Phys. Rev. Lett.* **2010**, *104*, 096804.

(29) Henkelman, G.; Uberuaga, B. P.; Jonsson, H. A. *J. Chem. Phys.* **2000**, *113*, 9901−9904.

(30) Cui, Y.; Fu, Q.; Bao, X. *Phys. Chem. Chem. Phys.* **2010**, *12*, 5053−5057.

(31) Vilkov, O.; Fedorov, A.; Usachov, D.; Yashina, L. V.; Generalov, A. V.; Borygina, K.; Verbitskiy, N. I.; Grüneis, A.; Vyalikh, D. V. *Sci. Rep.* **2013**, *3*, 2168.

(32) Zhou, H. T.; Mao, J. H.; Li, G.; Wang, Y. L.; Feng, X. L.; Du, S. X.; Mullen, K.; Gao, H. J. *Appl. Phys. Lett.* **2011**, *99*, 153101.

DOI: 10.1021/ja5113657
J. Am. Chem. Soc. XXXX, XXX, XXX−XXX